2013 IEEE International Conference on Robotics and Automation (ICRA)
Karlsruhe, Germany, May 6-10, 2013

Robust Real-Time Underwater Digital Video Streaming using Optical Communication

Marek Doniec
MIT, Cambridge, USA
doniec@mit.edu

Anqi Xu
McGill University, Montreal, Canada
anqixu@cim.mcgill.ca

Daniela Rus
MIT, Cambridge, USA
rus@csail.mit.edu

Abstract— **We present a real-time video delivery solution based on free-space optical communication for underwater applications. This solution comprises of AquaOptical II, a high-bandwidth wireless optical communication device, and a two-layer digital encoding scheme designed for error-resistant communication of high resolution images. Our system can transmit digital video reliably through a unidirectional underwater channel, with minimal infrastructural overhead. We present empirical evaluation of this system's performance for various system configurations, and demonstrate that it can deliver high quality video at up to 15 Hz, with near-negligible communication latencies of 100 ms. We further characterize the corresponding end-to-end latencies, i.e. from time of image acquisition until time of display, and reveal optimized results of under 200 ms, which facilitates a wide range of applications such as underwater robot tele-operation and interactive remote seabed monitoring.**

I. Introduction

Real-time transmission of live video is an essential component in a wide range of underwater applications, including the tele-operation of robotic vehicles and remote monitoring of underwater sensor stations. In this paper we present a novel system, operating via a free-space optical communication channel, that achieves wireless, real-time, and high-quality video delivery for underwater applications.

Conventionally, high quality underwater video streaming is implemented using tethered solutions [1], [2]. In such robot tele-control setups however, the tether restricts locomotion range, is prone to becoming tangled, and often requires human divers to wrangle the cable and prevent harming the underwater environment.

On the other hand, wireless communication methods face a different slew of obstacles in the aquatic domain, where for instance conventional electromagnetic, i.e. radio frequency (RF) based solutions are rendered infeasible due to heavy absorption of electromagnetic waves by water. Extensive research efforts have thus focused on transmitting video payloads via alternative communication channels such as acoustic technologies [3]. Unfortunately, the acoustic channel imposes inherent bandwidth restrictions and thus limits communication throughput to be on the order of 100 Kbps [4], [5]. Consequently, acoustic-based video streaming solutions are restricted to very low resolutions and slow frame rates, which makes them impractical for dexterous tele-manipulation tasks.

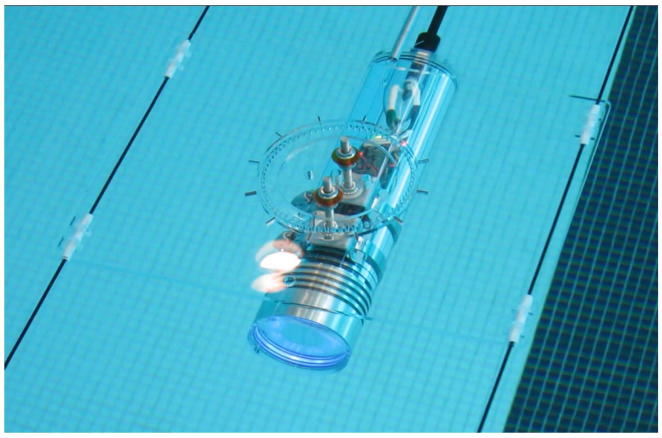

Fig. 1. AquaOptical II modem mounted on an underwater test rig.

In addition to advances in underwater acoustic communication technologies, a number of groups have recently begun exploring optical free-space communication as an alternative wireless transmission medium for aquatic settings. Cox *et al.* studied digital modulation over optical channels at data rates of 1 Mbps in a highly controlled test environment [6]. Simpson *et al.* investigated the use of (255,223) Reed-Solomon error correcting codes with a base transmission rate of 5 Mbps, and achieved communication distances of 7 m [7]. Anguita *et al.* presented an optical communication system with custom Physical and Media Access Control (MAC) network layers inspired by the 802.11 and 802.15.4 protocols. Their optical modem solution is deployed on a Field Programmable Gate Array (FPGA), and has a potential communication distance of up to 4 m [8]. Baiden *et al.* implemented an optical communication system with an omni-directional transmitter and receiver capable of achieving 1.5 Mbps throughput at 11 m distance in clear water environments [9]. Farr *et al.* conducted preliminary deployment of video transmission using an optical link at a data rate of 1 Mbps over a distance of 15 m [2].

In this paper, we introduce a state-of-the-art underwater video streaming solution that is comprised of a high-bandwidth wireless optical communication modem called AquaOptical II [10], and a two-layer digital encoding scheme designed for error-resistant communication of high definition images. Specifically, we employ (255,239) Reed-Solomon (RS) [11] inner code for byte-level error correction, coupled with a systematic Luby Transform (LT) [12] outer code to

978-1-4673-5643-5/13/$31.00 ©2013 European Union

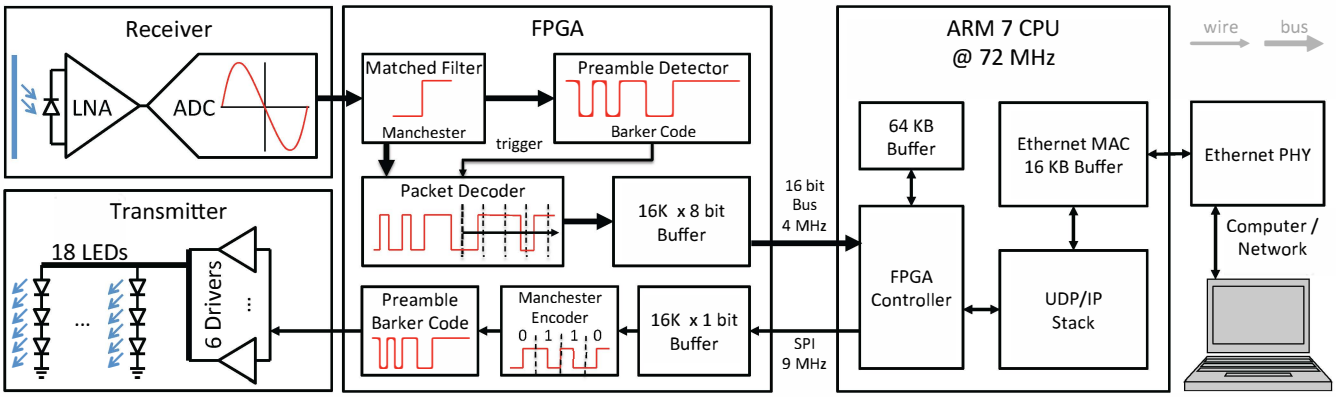

Fig. 2. The AquaOptical II modem [10] consists of a transducer compromising the `Receiver` and `Transmitter` units, an FPGA that implements the physical and link layer, and an ARM 7 CPU that implements the MAC layer and Ethernet communication.

mitigate packet-level losses. Our video transmission solution does not require feedback and can thus be used in a unidirectional communication channel with low infrastructural overhead. Our empirical assessments in clear water settings demonstrate the ability to stream video resolutions of up to 1288 $\times$ 964 pixels, deliver frame rates of up to 15 frames per second (FPS) robustly, and communicate at ranges of up to 40 m. We further show that this system can deliver 752 $\times$ 480 resolution video at 15 FPS with an average transmission latency of 100 ms and end-to-end latency of 170 ms, where the latter measure takes into account frame grabbing and image display delays.

This work contributes the following:

- a novel high-bandwidth underwater optical communication device;
- a two-layer digital encoding scheme which is highly robust to channel noise and also accommodates for unidirectional real-time streaming;
- extensive empirical results of the an end-to-end underwater video streaming solution.

Our video streaming solution is a key enabling technology for a wide range of underwater settings, including surveillance and robotics. We are especially interested in real time video transmission to enable such applications as video feed exchange among divers and live video delivery for surveillance networks. In addition, our high-bandwidth low-latency streaming solution plays a critical role in diverse underwater robotic applications, such as dexterous operations using Remotely Operated Vehicles (ROV), real-time telecontrol in narrow caves and shipwreck settings, and off-board visual autonomous navigation setups. The presented video streaming solution further complements our previous work, which demonstrated wireless remote control of an underwater vehicle using free-space optical communication [13].

The remainder of the paper is organized as follows: in Section II we present an overview of the AquaOptical II modem and the digital encoding algorithms. Section III describes our experimental methodology in evaluating this underwater video streaming solution. Experimental results are given in Section IV. We present a brief analysis of the results in Section V, and conclude in Section VI.

II. System Overview

This section provides an overview of our underwater video streaming solution between two AquaOptical II modems. The video feed is encoded on the transmitting computer in real time from images acquired by a digital camera. Once the data has been transmitted through the water medium via AquaOptical II, it is subsequently decoded on the receiving computer and is either analyzed by vision algorithms, or displayed to the user.

This section first elaborates on the AquaOptical II hardware and software, and then describes the video compression and two-layer encoding processes.

A. AquaOptical II

A system overview of the AquaOptical II modem [10] is shown in Fig. 2. This network interface can be decomposed into three different sections: (1) a transducer comprising the transmitter and receiver hardware, (2) an FPGA that implements the physical and link layers (as defined by the OSI network model), and (3) an ARM 7 CPU that handles the MAC layer and Ethernet communication. AquaOptical II is powered by an internal 86.6 Wh Lithium-Ion battery. It consumes up to 10 W when receiving data and an additional 30 W when transmitting data at full capacity. Receiver consumption scales roughly with incident light power and transmit power scales linearly with utilization.

The AquaOptical II modems receive and transmit payload data using the minimalistic User Datagram Protocol (UDP). The ARM CPU forwards all UDP packets received through the Ethernet interface of AquaOptical II to the FPGA and triggers a `packet transmit` signal. The FPGA then converts the raw bit stream into a transmit bit stream using Manchester coding, where a `0`-bit is encoded by a `01` sequence and a `1`-bit is encoded by a `10` sequence. The FPGA then pre-appends a 13-bit Barker code (binary: `1111100110101`), which is used by the receiver for packet detection and clock synchronization. The resulting transmit bit stream is then forwarded to the transmitter hardware at 8 MHz, and subsequently converted into current pulses that drive a series of Light Emission Diodes (LED).

The receiver hardware is comprised of an Avalanche photo-diode (APD), whose output signal is amplified by a low noise amplifier (LNA) and then digitized at a resolution of 12 bits and a rate of 32 mega-samples per second (MSPS). This stream is digitally convoluted by the FPGA on a per-sample basis to detect the packet preamble and to trigger the `packet decoder` finite state machine logic. Once the Barker code preamble is identified, a step function matched filter (with 8 samples width, to match an established maximum throughput rate of 4 Mbits) is used to decode the Manchester symbols, where the sign of the filter output is sampled into a binary value. The first 16 bits decoded this way are used to determine the length of the packet, and the remainder of the payload is subsequently stored in a buffer. Once the expected number of bits are sampled, the ARM CPU forwards the contents of the buffer as a UDP packet over Ethernet to the end user.

B. Video Frame Compression

In order to transmit high resolution video frames at fast frame rates, it is necessary to compress the video data before transmitting through the AquaOptical II modem. Inter-frame prediction-based video codecs, such as H.264 and Theora, can achieve very high compression ratios through the use of *predicted* image frames (P-frames) and *bi-predicted* frames (B-frames), which efficiently encode pixel content as relative changes to either previous frames, or previous and subsequent frames, respectively. When transmitting the compressed stream of frames over a noisy channel however, the loss of a single encoded frame will likely introduce significant visual artifacts in nearby frames as well. In addition, predictive frames often incur a significant latency during decoding, on the order of $\frac{1}{FPS}$, due to their inter-frame dependencies. Furthermore, these modern video codecs require a significant amount of computational power, and thus cannot sustain real-time software compression of high definition content. Specifically, our empirical testing using the `GStreamer` multimedia framework revealed that both H.264 and Theora codecs had difficulty encoding and decoding 1288×964 resolution images at 8 FPS on a high-end quad-core 2.5 GHz processor.

To achieve the goal of delivering real-time video content with minimal latency, we opted to use the comparably straight-forward Motion-JPEG (M-JPEG) codec, which operates by compressing individual frames separately using JPEG. Although this codec results in worse compression ratios compared to modern video codecs, its encoder and decoder both require minimal processing time, on the order of 5 ms in the worst case for 1288×964 pixel images. Therefore, using M-JPEG we were able to stream high quality video at fast rates of up to 15 Hz within the 4 Mbps bandwidth limit of the AquaOptical II modems. More importantly, the M-JPEG codec allows each received frame to be decoded immediately, and therefore avoids the inherent inter-frame latencies found in modern video codecs.

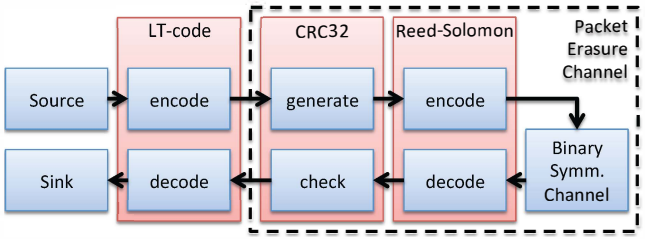

Fig. 3. Two-layer error coding scheme employed for high quality real-time video transmission via unidirectional free-space optical communication.

C. Video Frame Transmission

Fig. 3 illustrates a two-layer digital encoding scheme that we employed on AquaOptical II to robustly transmit high-volume framed content in a potentially noise-laden communication channel, with minimal transmission latency.

AquaOptical II is driven by an oscillator clock source with a frequency stability of 50 parts per million (ppm). This consequently limits the maximum packet size in burst transmission to be a few hundred bytes, in order to avoid de-synchronization errors due to clock drifts. To accommodate this, each video frame is converted into a sequence of fixed-sized fragments by AquaOptical II prior to transmission. This has the benefit of restricting the scope of transmission errors, in that if a single fragment is lost or corrupted, only that fragment needs to be recovered, rather than having to recover the entire frame.

We employed Luby Transform (LT) codes, a form of digital fountain codes, to ensure robust transmission of each video frame. LT codes operate by splitting a large payload into N equal-sized blocks, and then generating a theoretically infinite stream of packets, which we call fragments, by convolving one or more of these blocks together. It can be shown that the reception of any subset of size $\geq (1+\epsilon) \cdot N$ of these fragments allows for the recovery of the original frame with high probability. In addition to placing only a constraint on the number of fragments received, but not on which fragments exactly, this approach also does not require feedback from the receiver, and hence allows our video streaming solution to be unidirectional. Furthermore, this allows the bandwidth of AquaOptical II to be fully utilized in a real-time streaming context, since the system can continue to transmit further different fragments until the next video frame is available. Our implementation uses a variant called systematic LT codes [12], where the first N fragments transmitted are the single blocks from the source frame, and subsequent fragments are generated pseudo-randomly based on the fragment ID.

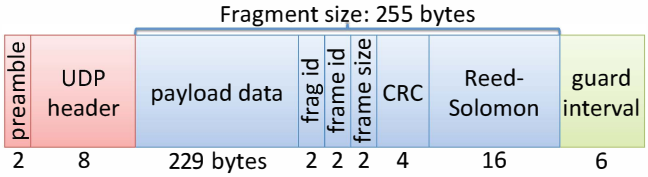

Fig. 4. Structure of packets sent by the AquaOptical II modem.

The 255-bytes packet structure for AquaOptical II is shown in Fig. 4, and contains both the payload fragment data, as well as the fragment ID, the frame ID, and the total size of the frame. In addition, we generate a 4 byte cyclic redundancy check (CRC) from the fragment payload, and then encode the entire packet using (255,239) Reed-Solomon (RS) error correcting code, which can recover up to 8 bytes of error per packet. By accounting for the preamble, UDP header, packet data, and the guard interval, each packet takes a total of $547\ \mu s$ to transmit using AquaOptical II. Our video streaming solution configured the LT encoder to send a new packet to the modem every $560\ \mu s$, thus resulting in 1785 fragments being transmitted per second.

AquaOptical II's coding scheme, as depicted in Fig. 3, implements a binary symmetrical channel, where noise-induced bit-flips occur with a probability p. This probability depends on the receiver's signal strength, which in turn is affected by factors such as transmission distance and water turbidity. By using a Reed-Solomon code in combination with a CRC we are turning this binary symmetrical channel into a packet erasure channel, in which entire packets are either lost (the errors cannot be recovered and the CRC fails) or successfully decoded with very high probability (where the CRC passes). The use of an LT code makes it highly likely that a frame can be recovered as soon as enough fragments have been received, thus keeping latency low.

III. Experimental Methodology

We evaluated our underwater transmission system by measuring the performance of its live video transmission in different settings. We deployed AquaOptical II modems in two indoor pools of 25 m and 50 m lengths, and streamed live video feeds at 0.5 m depth using a cabled test rig, as shown in Fig. 5. In these setups, the video source was obtained from natural pool scenes while targetting at the AMOUR robot, and was captured using a waterproof USB camera connected to a laptop computer. The encoded video fragments were sent out as UDP packets from a stationary AquaOptical II modem positioned against the pool wall. A second AquaOptical II modem, mounted on a movable cart positioned along the 1-D track, received these packets and forwarded them to the recipient computer for decoding, analysis, and logging.

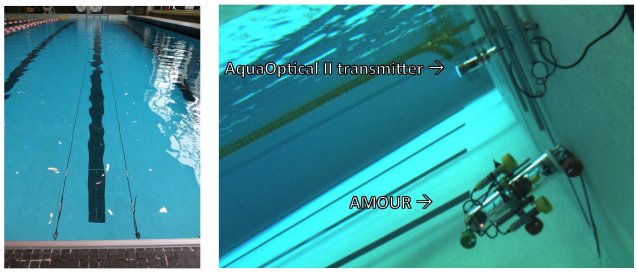

(a) Cabled test rig (b) Acquired camera frame

Fig. 5. Our experiment testbed consists of two AquaOptical II modems attached to carts and mounted facing each other on a cabled test rig in an indoor pool (a). Live video feed of the underwater AMOUR robot were streamed through the setup during our tests (b).

Our pool trials consisted of over 70 video streaming runs, corresponding to over 30,000 frames transmitted in total, while varying different system parameters. These parameters included the image resolution, video frame rate, JPEG compression quality, and modem-to-modem distance. We computed the following metrics on our collected data to thoroughly characterize the performance of the resulting video transmissions:

- *frame success rate*: percentage of successfully decoded frames;
- *frame latency*: time delay for transmitting a raw RGB image from one computer to another through the encoded optical channel;
- *peak signal-to-noise ratio (PSNR) [14]*: non-subjective measure of image quality between the compressed transmitted feed and the raw source image;

Furthermore, the collected video transmission data was also used to evaluate the performance of our digital encoding scheme for transmitting general purpose payloads over a potentially noisy free-space optical channel.

Fig. 6. Sample acquired camera frame during our benchtop trial, used to determine the end-to-end video capture-transmission-display latency.

In addition to characterizing the transmission performance of individual video frames, we are also interested in studying the overall performance of live video feeds using the proposed underwater streaming solution. This is motivated by a number of applications, such as remote visual monitoring of underwater sensor stations, and visual-guided tele-operation of underwater robotic vehicles. To this end, we repeated our video streaming experiments in a controlled benchtop environment, where two AquaOptical II modems were positioned next to each other in free space. This is comparable to our underwater setup since we had empirically confirmed that the AquaOptical II hardware exhibited near identical latencies and packet drop rates both in an underwater pool setting and above water. This close-range analogue enabled us to aim the camera at the recipient computer's monitor, which displayed both the latest decoded frame as well as a high-resolution stopwatch operating at the computer display refresh rate of 60 Hz, as shown in Fig. 6. Thus, the recorded camera frames revealed the *end-to-end video latency*, namely the time delay between capturing a camera frame and displaying on the recipient's monitor, which is one of the essential statistics of video streaming applications.

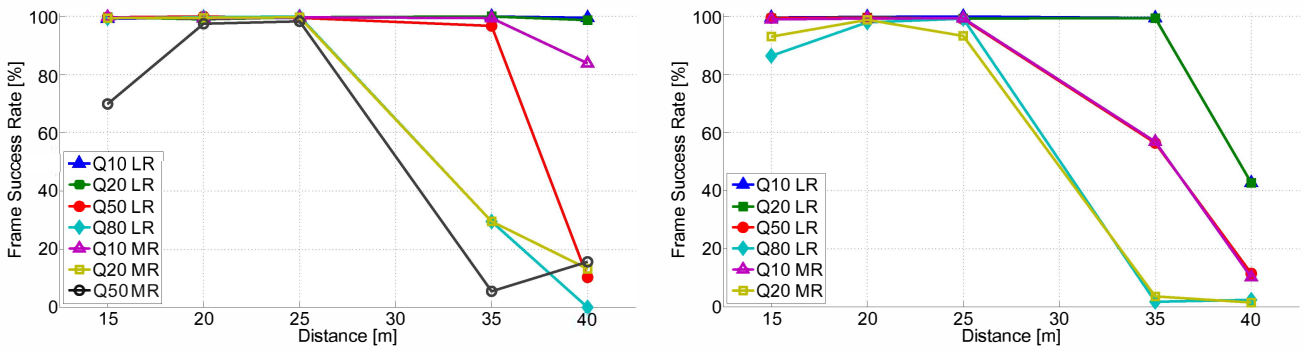

(a) vs. distance, 10 FPS

(b) vs. distance, 15 FPS

Fig. 7. Reception success rates for all transmitted frames for different video qualities, plotted against modem-to-modem distance.

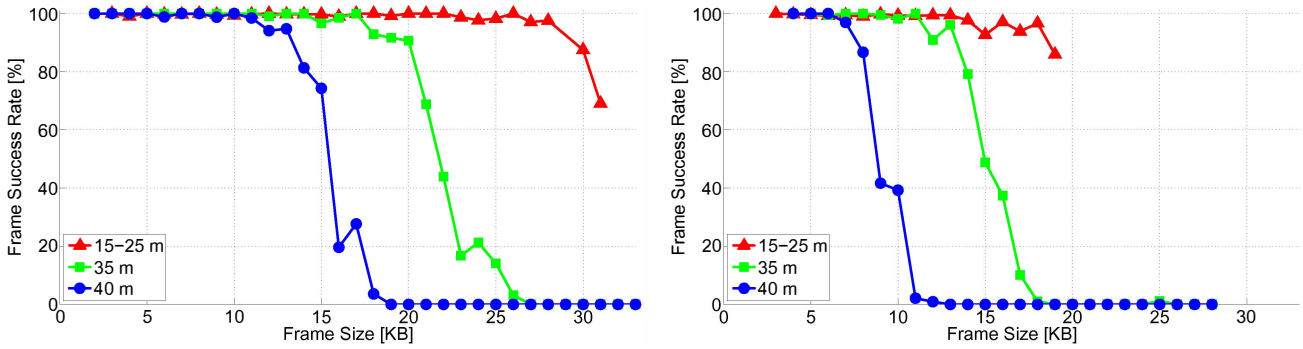

(a) vs. compressed frame size, 10 FPS

(b) vs. compressed frame size, 15 FPS

Fig. 8. Reception success rates for all transmitted frames at different modem-to-modem distances, plotted against frame size (in 1 KB bins).

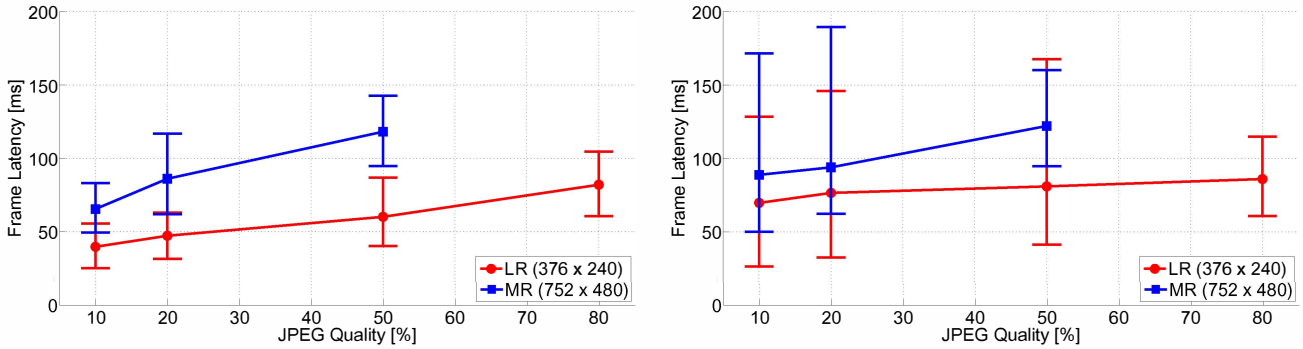

(a) Close range (15-25 m)

(b) Far range (35-40 m)

Fig. 9. Frame latency at different ranges, as a function of JPEG quality. Vertical bars depict 5% and 95% percentiles.

In our pool experiments we used the FireFly MV CMOS USB 2.0 camera (FMVU-03MTC), and in benchtop trials we also used FireFly, as well as the Flea 3 CCD Gigabit Ethernet camera (FL3-GE-13S2C), both commercially available from PointGrey technologies[1]. Both cameras were equipped with global shutters, and produced raw Bayer-encoded images, which were then converted into RGB colorspace prior to applying the M-JPEG video codec. The FireFly MV camera was configured to grab frames of 752×480 pixel resolution at 60 Hz capture rate, and the Flea 3 camera was configured to grab 1288×964 pixel images at 30 Hz. Using these sources, we carried out video streaming sessions at three different image resolutions:

- Low resolution (LR): 376×240 pixels
- Medium resolution (MR): 752×480 pixels
- High resolution (HR): 1288×964 pixels

IV. Experimental Results

The success rate of receiving JPEG frames in our video streaming pool trials are plotted as a function of modem distance in Fig. 7, and as a function of frame size in Fig. 8. For the received JPEG frames, Fig. 9 depicts the frame transmission latencies as a function of the JPEG compression quality, for both close ranges of within 25 m and far ranges of up to 40 m. This compression quality ratio is proportionally correlated to the size of each encoded frame, and separately to the PSNR image qualities, as shown in Fig. 10.

[1]www.ptgrey.com

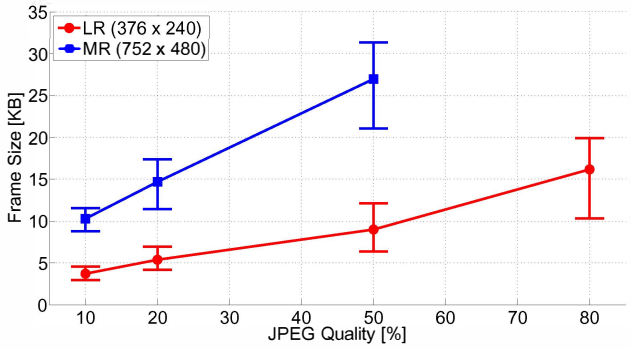

(a) Frame Size vs. JPEG Quality

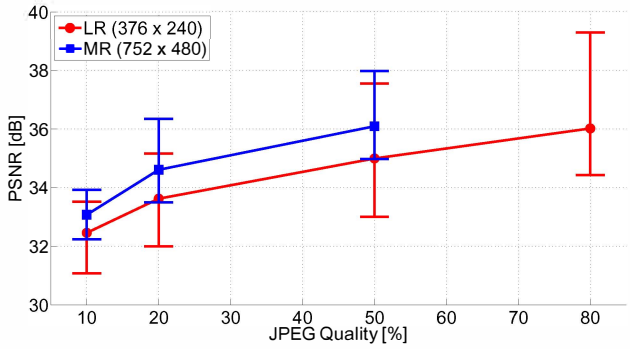

(b) PSNR vs. JPEG Quality

Fig. 10. Image properties for the video streams used in the pool experiment, as a function of JPEG quality. Vertical bars depict 5% and 95% percentiles.

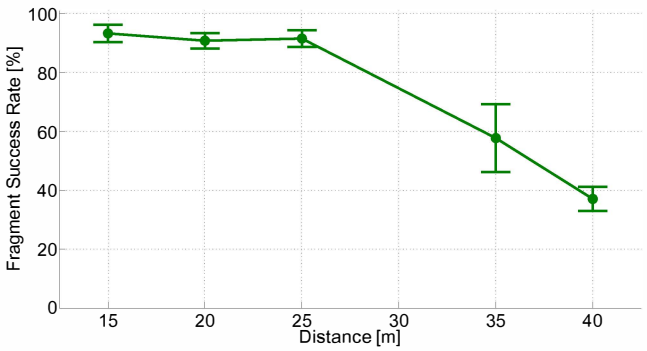

Fig. 11. Reception success rates for all transmitted fragment instances for all pool trials, vs. distance. Vertical bars depict $\pm 1\sigma$.

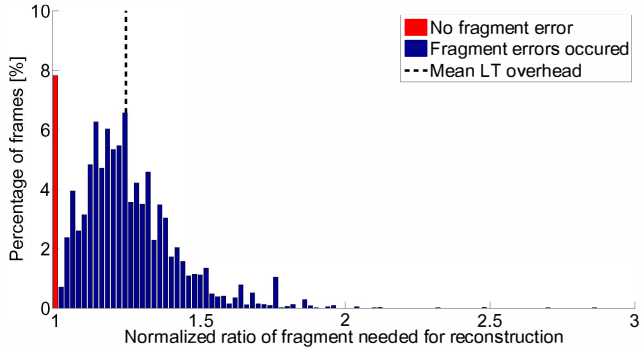

(a) Close range (25 m)

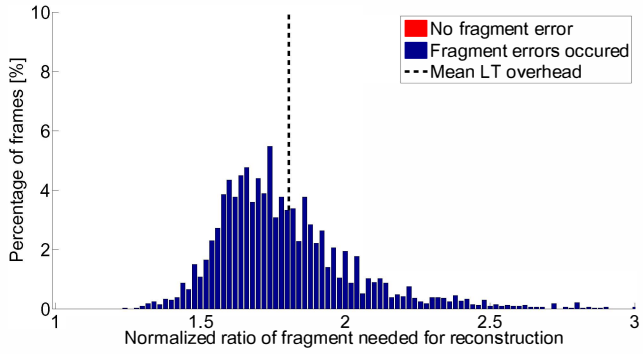

(b) Far range (35 m)

Fig. 12. Ratio of the number of fragments received at a fixed range before a frame can be decoded, over the number of systematic fragments for the frame, representing LT overhead. The red bar on the left side of the plot represents instances where the frame was immediately decoded after successfully receiving the initial N systematic fragments.

Focusing on the performance of the two-layer RS / LT encoding scheme, Fig. 11 depicts the percentage of fragments successfully decoded as a function of modem distance. Fig. 12 illustrates the overhead required by the systematic LT outer code to reconstruct the frame. This overhead is measured as the ratio between the number of total fragments received before the frame could be decoded, normalized over the number of systematic fragments, N, for the source image frame. These overhead results are aggregated into a plot of the expected LT overhead as a function of the distance, in Fig. 13.

Looking at the packet level, Fig. 14 shows histograms of the time intervals between received fragment packets, both for near and far ranges. The *expected* bandwidth of our underwater optical transmission system at different ranges can be computed as the ratio of the averaged inter-packet interval, divided by the total volume of packet data transmitted during this duration. This expected bandwidth can also be determined by multiplying the fragment reception success rate, in Fig. 11, with AquaOptical II's maximum transmission bandwidth of 4 Mbps.

The end-to-end latencies measured during our benchtop tests are shown in Fig. 15. We have further determined that the gap between the frame transmission latency and the end-to-end latencies for our hardware setups are on average 60 ms for low-resolution and medium-resolution images, and 200 ms for high-resolution images. This increase in latency accounts for the duration of grabbing a camera frame, converting it into RGB colorspace, and displaying the received RGB image on the recipient's monitor. These values are useful because they can be added to our latency results in Fig. 9 to obtain the corresponding expected end-to-end latencies for our pool trial sessions, since neither the frame grabbing delay nor the image display duration are dependent on the communication medium used to transmit these frames.

V. Discussion

The parameter values used in our experiments are representative of typical video streaming settings, and were chosen to be of equal or better quality compared to similar

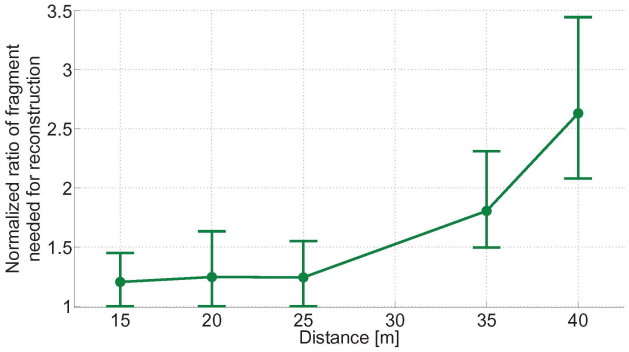

Fig. 13. LT overhead as a function of modem ranges. Vertical bars depict 5% and 95% percentiles.

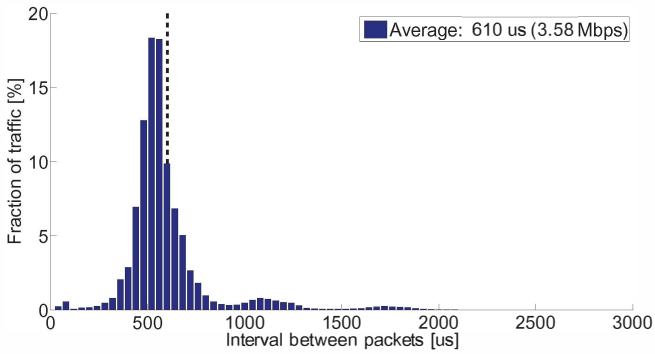

(a) Close range (15-25 m)

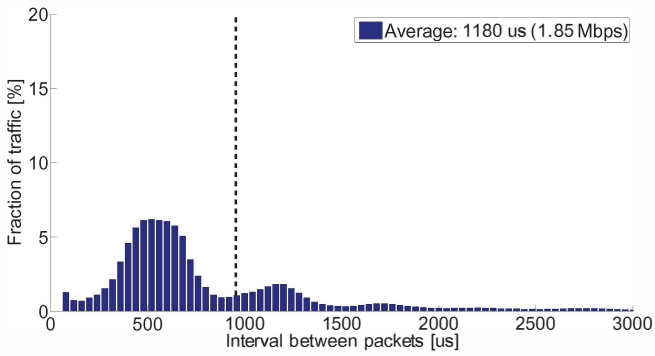

(b) Far range (35-40 m)

Fig. 14. Histogram of time intervals between consecutive fragments received. Peaks in each histogram are centered around integer multiples of the transmitter's packet delay of 560 μs.

studies conducted in the robotics literature. In particular, we observed anecdotally that images with JPEG compression qualities varying from 10% to 80% produced images that were subjectively rated as passably-visible to great quality, respectively. In addition, as shown in Fig. 10(b), these compressed images resulted in PSNR values above 30 dB, which is conventionally considered to be of decent quality [15], [14]. Similarly, our selection of frame rates and image resolutions provide competitive video accuracy compared to previous studies involving video streams [16], [17].

Fig. 7 revealed that all of the tested video settings have resulted in near perfect frame success rates within 25 m. In addition, configurations that yielded relatively small-sized frames have been shown to be robust at even greater

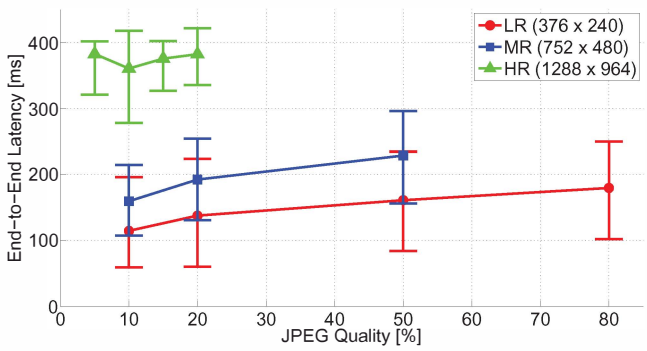

Fig. 15. End-to-end latencies for capturing real-time video, streaming it via an unidirectional underwater free-space optical channel, and displaying the feed on a recipient computer. Vertical bars depict 5% and 95% percentiles.

distances, where the optical signal degradation were far more pronounced. Since the frame success rate is directly influenced by the underlying fragment success rate, it is not surprising that Fig. 7 and Fig. 11 depict similar-shaped curves. Nevertheless, the various frame success rate curves showed consistently steeper drop offs compared to the fragment success rate curve, which is attributed to the relatively strict maximum duration during which each video frame can be decoded, before the transmitter starts sending fragments corresponding to the subsequent frame.

By plotting the frame success rate as a function of the frame size in Fig. 8, we provide an indication of the expected transmission rates for framed data in general, and not necessarily just video frames. In particular, although our current system uses M-JPEG codec, which generates consistently-sized frames, the results in Fig. 8 can be used to predict the expected performance of variable-bitrate framed content such as videos encoded with inter-frame codecs like H.264 or Theora, or multi-modal content, for example high-bandwidth payload interleaved with low-bandwidth status and signaling meta-data in robot tele-operation applications.

Overall, our various video streaming tests showed similar performances at close ranges of up to 25 m, and also showed similar degradations as the distance between the two modems increased. This performance discrepancy can also be seen from the LT overhead plots, where for instance a noticeably more significant portion of frames were decoded using only the first N systematic fragments at close ranges (i.e. the red bar in Fig. 12(a)). The difference in the two ranges can further be attributed to the expected amount of packets dropped in Fig. 11, and in particular, in Fig. 14(a) the large peak around 560 us time interval indicates that a large percentage of fragments were received by the decoder at

Resolution	Frame rate	JPEG quality	PSNR	Frm. latency	Frame size
374 x 240	15 fps	80	37.0 dB	74.9 ms	13.4 KB
752 x 480	15 fps	20	34.7 dB	102.7 ms	14.7 KB
752 x 480	10 fps	50	36.3 dB	116.0 ms	26.4 KB
1288 x 964	8 fps	20	38.6 dB	134.9 ms	33.2 KB

Fig. 16. Summary of underwater compressed video streaming results for several representative video settings.

close ranges, whereas at farther distances (Fig. 14(b)) the distribution of fragments shifted to the second and third peaks, at twice and thrice the transmission interval, and consequently indicating the loss of one and two fragments, respectively.

A summary of the performance of our video streaming solution for several representative system configurations can be found in Fig. 16. These indicate that our system can achieve frame transmission latencies of under 135 ms, and corresponding end-to-end latencies between 170 ms and 400 ms. These suggest that our video streaming solution is capable of enabling a range of high-performance underwater applications based on various latency studies, including visual monitoring ([17], 300 ms), interaction with virtual environments ([18], 225 ms; [19], 313 ms), tele-surgery ([20], 250 ms), and tele-operated robotics ([21], 460 ms).

VI. Conclusion

This paper described a real-time and robust video streaming solution for underwater applications. We devised and integrated two-layer forward error correction scheme, consisting of an inner RS code and an outer LT code. This scheme allows for robust video transmission via an unidirectional underwater channel. We further presented the latest iteration of our in-house developed optical modem technology, AquaOptical II, which complements our error correction scheme in achieving real-time robust underwater video transmission. To the best of our knowledge, the empirical results presented in this work provide leading latency and image quality standards for underwater video streaming. Furthermore, these results suggest that our real-time video transmission solution can be integrated in a wide range of underwater applications, such as robot tele-operation and remote monitoring, to deliver high-performance experiences, according to a number of empirical studies in the literature.

In future work we would like to augment the system with hardware-based video compression capabilities in order to further increase the range of frame resolution and quality afforded by our underwater video streaming solution. We are also investigating the integration of this video streaming solution along with a tele-control system for AUVs, to close the loop between the user and the robot. Finally, using a bi-directional communication channel would further allow us to dynamically optimize system parameters based on the current link quality and available bandwidth.

VII. ACKNOWLEDGMENTS

Support for this research has been provided in part by the MURI Antidote grant N00014-09-1-1031 and NSF grants IIS-1133224 and IIS-1117178. Anqi Xu was funded by the Vanier Canada Graduate Scholarship and the Michael Smith Foreign Study Supplement. We are grateful for this support. We are grateful to Michael Angermann, Afian Anwar, Michael Glombicki, Daniel Hawkins, Daniel Soltero, and Mikhail Volkov whose help with the logistics of conducting our pool experiments have been invaluable.

References

[1] G. Dudek, M. Jenkin, C. Prahacs, A. Hogue, J. Sattar, P. Giguere, A. German, H. Liu, S. Saunderson, A. Ripsman, S. Simhon, L.-A. Torres, E. Milios, P. Zhang, and I. Rekletis, "A visually guided swimming robot," in *Proc. of the IEEE/RSJ Int. Conf. on Intelligent Robots and Systems (IROS '05)*, 2005, pp. 3604–3609.

[2] N. Farr, A. Bowen, J. Ware, C. Pontbriand, and M. Tivey, "An integrated, underwater optical / acoustic communications system," in *IEEE OCEANS Sydney 2010*, 2010.

[3] C. Pelekanakis, M. Stojanovic, and L. Freitag, "High rate acoustic link for underwater video transmission," in *OCEANS 2003*, 2003, pp. 1091–1097.

[4] D. Kilfoyle and A. Baggeroer, "The state of the art in underwater acoustic telemetry," *Oceanic Engineering, IEEE Journal of*, vol. 25, no. 1, pp. 4 –27, jan 2000.

[5] I. F. Akyildiz, D. Pompili, and T. Melodia, "Underwater acoustic sensor networks: Research challenges," *Ad Hoc Networks*, vol. 3, pp. 257–279, 2005.

[6] W. Cox, J. Simpson, and J. Muth, "Underwater optical communication using software defined radio over led and laser based links," in *Military Communications Conference (MILCOM '11)*, 2011, pp. 2057–2062.

[7] J. Simpson, W. Cox, J. Krier, B. Cochenour, B. Hughes, and J. Muth, "5 mbps optical wireless communication with error correction coding for underwater sensor nodes," in *OCEANS 2010*, 2010.

[8] D. Anguita, D. Brizzolara, and G. Parodi, "Optical wireless communication for underwater wireless sensor networks: Hardware modules and circuits design and implementation," in *OCEANS 2010*, 2010.

[9] G. Baiden and Y. Bissiri, "High bandwidth optical networking for underwater untethered telerobotic operation," in *OCEANS 2007*, 2007.

[10] M. Doniec, C. Detweiler, I. Vasilescu, M. Chitre, M. Hoffmann-Kuhnt, and D. Rus, "Aquaoptical: A lightweight device for high-rate long-range underwater point-to-point communication," *Marine Technology Society Journal*, vol. 44, no. 4, pp. 55–65, July/August 2010.

[11] I. S. Reed and G. Solomon, "Polynomial codes over certain finite fields," *Journal of the Society for Industrial and Applied Mathematics*, vol. 8, no. 2, pp. 300–304, 1960.

[12] T. Nguyen, L.-L. Yang, and L. Hanzo, "Systematic luby transform codes and their soft decoding," in *Proc. of the IEEE Workshop on Signal Processing Systems (SiPS '07)*, 2007, pp. 67–72.

[13] M. Doniec, C. Detweiler, I. Vasilescu, and D. Rus, "Using optical communication for remote underwater robot operation," *iuliucom*, pp. 4017–4022, 2010.

[14] S. Welstead, *Fractal and Wavelet Image Compression Techniques*. SPIE Publications, 1999.

[15] P. Piñol, M. Martinez-Rach, O. Lopez, M. Malumbres, and J. Oliver, "Analyzing the impact of commercial video encoders in remotely teleoperated mobile robots through ieee 802.11 wireless network technologies," in *Proc. of the 5th IEEE Int. Conf. on Industrial Informatics*, 2007, pp. 425–430.

[16] B. O'Brien and J. Kovach, "Underwater wireless optical communication channel modeling and performance evaluation using vector radiative transfer theory," *IEEE Journal on Selected Areas in Communications*, vol. 26, no. 9, pp. 1620–1627, 2008.

[17] L. Zuo, J. G. Lou, H. Cai, and J. Li, "Multicast of real-time multi-view video," in *Proc. of the 2006 IEEE Int. Conf. on Multimedia and Expo*, 2006, pp. 1225–1228.

[18] I. S. MacKenzie and C. Ware, "Lag as a determinant of human performance in interactive systems," in *Proc. of the INTERACT / CHI conference on human factors in computing systems (INTERCHI '93)*, 1993, pp. 488–493.

[19] S. R. Ellis, M. J. Young, B. D. Adelstein, and S. M. Ehrlich, "Discrimination of changes in latency during head movement," in *Proc. of the 8th Int. Conf. on Human-Computer Interaction (HCI '99)*, 1999, pp. 1129–1133.

[20] M. Lum, J. Rosen, H. King, D. Friedman, T. Lendvay, A. Wright, M. Sinanan, and B. Hannaford, "Teleoperation in surgical robotics - network latency effects on surgical performance," in *Proc. of the IEEE Int. Conf. on Engineering in Medicine and Biology Society (EMBC '09)*, 2009, pp. 6860–6863.

[21] B. Ross, J. Bares, D. Stager, L. Jackel, and M. Perschbacher, "An advanced teleoperation testbed," in *Field and Service Robotics*, ser. Springer Tracts in Advanced Robotics, vol. 42, 2008, pp. 297–304.